Monthly Notices of the ROYAL ASTRONOMICAL SOCIETY

MNRAS **538,** 963–975 (2025) https://doi.org/10.1093/mnras/staf331
Advance Access publication 2025 February 22

Subhaloes are anisotropically distributed and aligned with the smooth matter distribution of their host haloes

Lorena Mezini [1]★ Andrew R. Zentner [1,2] Kuan Wang [3,4] and Catherine Fielder [5]

[1]*Department of Physics and Astronomy, University of Pittsburgh, Pittsburgh, PA 15260, USA*
[2]*Pittsburgh Particle Physics, Astrophysics, and Cosmology Center (PITT PACC), University of Pittsburgh, Pittsburgh, PA 15260, USA*
[3]*Department of Physics, University of Michigan, Ann Arbor, MI 48109, USA*
[4]*Leinweber Center for Theoretical Physics, University of Michigan, Ann Arbor, MI 48109, USA*
[5]*Steward Observatory, University of Arizona, 933 North Cherry Avenue, Rm. N204, Tucson, AZ 85721-0065, USA*

Accepted 2025 February 14. Received 2025 February 14; in original form 2024 June 14

ABSTRACT

We investigate the distributions of subhaloes about their hosts in two suites of zoom-in *N*-body simulations of halo growth – one suite focused on Milky Way-Mass haloes ($\sim 10^{12}$ M$_\odot$) and another focused on cluster-mass haloes ($\sim 10^{15}$ M$_\odot$) in the Symphony simulation suite. We find, in agreement with previous work on this subject, that subhaloes are distributed anisotropically about their host haloes. In particular, the positions of subhaloes lie preferentially near the major axes of their host haloes, possibly implying that satellite galaxies will exhibit a similar alignment. Furthermore, we show that in two-dimensional projection subhaloes are more likely to be observed near the halo centre (where the central galaxy presumably resides) when the host halo is projected nearly along its major axis. This projection effect is significant. Within projected radii of a few per cent of the virial radius of the host halo, the fraction of mass in subhaloes is ~ 175 per cent larger for Milky Way-mass haloes and as much as ~ 195 per cent larger for cluster haloes when projected along the major axis as compared to the average from a random projection. This result has consequences for many applications including the interpretation of gravitational lenses. Finally, we find that the orbital angular momentum vector of subhaloes is aligned with the angular momentum vector of their host halo, indicating that a significant component of a halo's angular momentum may be carried in its subhaloes. This has consequences for galaxy formation models which use host halo angular momentum as a proxy for galaxy momentum.

Key words: gravitational lensing: strong – galaxies: clusters: general – galaxies: haloes – dark matter – large-scale structure of Universe.

1 INTRODUCTION

The contemporary galaxy formation paradigm holds that galaxies form within the potential wells supplied by haloes of dark matter (White & Rees 1978; Blumenthal et al. 1984). In the standard ΛCDM (cold dark matter with a cosmological constant) model of the Universe, dark matter haloes form when perturbations in the initial matter field collapse into gravitationally bound objects. These structures grow by the accretion of mass from surrounding dark matter and through mergers with other haloes; smaller haloes that are not entirely disrupted upon merging with a larger halo are known as subhaloes (see e.g. Kauffmann, White & Guiderdoni 1993; Klypin et al. 1999; Moore et al. 1999; Taylor & Babul 2002, 2004; Zentner & Bullock 2003; Zentner et al. 2005a; Bullock 2010; Jiang & van den Bosch 2016; van den Bosch & Jiang 2016).

ΛCDM predicts the existence of subhaloes on all mass scales. Some alternative models for dark matter predict differing amounts of substructure. Warm dark matter has become the benchmark example of an alternative to CDM that predicts less substructure in general and fewer subhaloes in particular (e.g. Colín, Avila-Reese & Valenzuela 2000; Bode, Ostriker & Turok 2001; Lovell et al. 2014). However, various alternatives to CDM make distinct predictions for the structure and abundance of dark matter, including self-interacting dark matter (e.g. Tulin & Yu 2018), fuzzy dark matter (e.g. Hui 2021), and decaying dark matter (e.g. Peter & Benson 2010; Wang et al. 2013, 2014). Consequently, the observation (or non-observation) of subhaloes within larger host haloes can be used as a test of dark matter.

One tool for detecting dark matter substructure is strong gravitational lensing – a phenomena that takes place when a massive foreground object, such as a dark matter halo and the galaxy that it contains, deflects the light of a background luminous object, such as a galaxy or quasar. For strong lensing to occur, the two-dimensional projected density of the 'lens' must be greater than a critical density. This threshold is often only reached in the area near the centres of haloes with size defined by the *Einstein radius*. For substructure lensing to occur, in particular, the projected positions of subhaloes must be near the scale of the Einstein radius. For example, lensing by substructure has been noted in multiply imaged systems (Meneghetti et al. 2006; Alard 2008; Hezaveh et al. 2016) as well as arc systems (Mao & Schneider 1998; Metcalf & Madau 2001; Bradač et al.

★ E-mail: lom31@pitt.edu

2002; Chiba & Takahashi 2002; Dalal & Kochanek 2002; Metcalf & Zhao 2002; Keeton 2003; Metcalf et al. 2004; Oguri et al. 2012). If subhaloes are distributed anisotropically with respect to their host haloes, it is more likely that subhaloes will fall in close proximity to the Einstein radius when a halo is viewed at a specific orientation. In other words, the probability of lensing by substructure is not uniform, but instead is biased by halo shape and halo orientation. The goal of this work is to explore the anisotropic distribution of subhaloes about their host haloes as a prelude to forthcoming studies of strong gravitational lensing. However, the anisotropic distributions of subhaloes (and, by assumption, of satellite galaxies) about their hosts can have consequences for many kinds of observations, some of which we discuss briefly below.

A significant body of work predicts that subhaloes in CDM simulations of structure formation should be distributed anisotropically about their host haloes. Host dark matter haloes are ellipsoidal in shape (Barnes & Efstathiou 1987; Dubinski & Carlberg 1991; Warren et al. 1992; Dubinski 1994; Tormen 1997; Thomas et al. 1998; Jing & Suto 2002; Springel, White & Hernquist 2004; Hopkins, Bahcall & Bode 2005), and in particular, haloes tend to be prolate ellipsoids. Zentner et al. (2005b) found preferential alignments between the overall mass distribution of Milky Way-mass host haloes and the spatial distribution of their subhaloes, and this was confirmed in galaxy formation simulations shortly thereafter (Libeskind et al. 2007). More recently, Karp, Lange & Wechsler (2023) find an overdensity of satellite galaxies along the major axis of their central galaxy in the IllustrisTNG simulation. It is believed that these phenomena are the result of haloes preferentially merging along filaments in the large-scale structure (Wang et al. 2005; Zentner et al. 2005b; Libeskind et al. 2007; Libeskind et al. 2010; Kang & Wang 2015; Libeskind et al. 2015; Shi, Wang & Mo 2015; Shao et al. 2018; Morinaga & Ishiyama 2020). These filaments trace out preferred directions about haloes in the large-scale structure. Several simulations have found that alignments between neighbouring dark matter haloes tend to take place along the direction of the longest axes (the major axes) of the haloes. Faltenbacher et al. (2002) and Hopkins et al. (2005) detect alignments between the major axes of cluster-sized haloes out to separations of approximately 100 and 30 h^{-1} Mpc, respectively. Using the IllustrisTNG simulation, Rodriguez, Merchán & Artale (2024) report alignments out to 10 h^{-1} Mpc for both the stellar and dark matter components of galaxies.

The prediction that subhaloes are distributed anisotropically about their hosts and that they are aligned preferentially with the non-spherical dark matter distribution of their hosts has some observational support from a variety of analyses of galaxies from surveys such as the Sloan Digital Sky Survey (SDSS). Using a sample of galaxy groups from SDSS DR4, Brainerd (2005) and Yang et al. (2006) showed that satellites tend to be aligned with the major axis of the central galaxy in the group. Azzaro et al. (2007) reached qualitatively similar conclusions for the SDSS DR4 sample using complementary methods (see also Azzaro et al. 2006). Wang et al. (2018) and Rodriguez, Merchán & Artale (2022) performed a similar analyses using SDSS DR7 and SDSS DR16 data, respectively, and found that this alignment exists primarily between red central galaxies and their red satellites. More recently, Samuels & Brainerd (2023) showed that satellite distributions tend to be lopsided with satellites preferentially residing on one side of their host in agreement with Libeskind et al. (2016) and Brainerd & Samuels (2021). Similar results have been observed in cluster lensing analyses. Using SDSS, Evans & Bridle (2009) determined that dark matter haloes are preferentially aligned in the same direction as indicated by the spatial distribution of cluster galaxies using cluster lensing. Gonzalez et al. (2021) drew similar conclusions from a galaxy lensing analysis of a number of surveys.

In contrast to the large-scale structure survey analyses mentioned above, satellites of the Milky Way and M31 Galaxies have been observed to preferentially lie in a plane *perpendicular* to their host galaxy major axis (Kunkel & Demers 1976; Lynden-Bell 1976; Majewski 1994; Grebel 1999; Mateo 1998; Hartwick 2000; Willman et al. 2004; Kroupa, Theis & Boily 2005; Metz et al. 2009; Pawlowski, Pflamm-Altenburg & Kroupa 2012; Conn et al. 2013; Ibata et al. 2013). This particular alignment of satellites has been dubbed the *Holmberg Effect* and was first described in Holmberg (1969). Aside from the fact that these Local Group measurements refer to only two central galaxies, there are other differences between the Holmberg Effect in the Local Group and the SDSS measurements. First, and foremost, the central galaxies of the Local Group are both disc galaxies, whereas the statistics of the SDSS measurements were dominated by elliptical galaxies. Secondly, the Milky Way and M31 form a close pair of galaxies and it is uncertain the degree to which alignment effects may be enhanced or reduced in close pair systems.

In addition to the biases in the angular distributions of subhaloes about their host galaxies, subhaloes may also be kinematically biased relative to the smooth dark matter component in their hosts. These biases may be relevant in studies of galaxy formation. In models of disc galaxy formation, the central disc galaxy acquires its angular momentum from its host halo (Navarro & Benz 1991; Navarro & White 1993; Navarro & Steinmetz 1997; D'Onghia et al. 2006; Kaufmann et al. 2007). For this reason, host halo angular momentum is often used as a proxy for galaxy angular momentum in semi-analytical galaxy formation models (Somerville et al. 2008; Benson 2012). However, the influence of subhaloes on angular momentum must not be overlooked in these models. Subhaloes that merge from coherent directions, such as along filaments, often have angular momenta that are aligned with the angular momentum of their host halo (Aubert, Pichon & Colombi 2004). However, it is not clear that the angular momentum carried by the subhaloes should be included in the available reservoir of angular momentum that can be conveyed to the central disc galaxy. If it is the case that subhaloes carry more angular momentum per mass than hosts in general and that subhalo angular momentum displays some preferred alignment with the host halo, this could induce a bias in models that estimate the amount of halo angular momentum transmitted to the baryonic disc. Whether or not the subhaloes represent a distinct population and whether or not they represent the angular momentum of typical host particles should be accounted for in such models.

In this paper, we revisit the question of the degree to which the positions and momentum of subhaloes within host haloes are aligned with the mass distribution of their hosts, particularly, whether or not subhaloes are preferentially aligned with the principle axes and angular momenta of their hosts. As will be evident, the primary application we have in mind is strong gravitational lensing, though we have attempted to summarize results in such a way as to be useful for a variety of other applications. This paper is organized as follows. In Section 2 of this paper, we discuss the simulations used, Section 3 introduces the various halo properties that we studied, and in Section 4 and Section 5 we go over the alignment results for host haloes and host-sub halo alignments, respectively. Finally, we discuss our results and draw conclusions in Section 6.

2 SIMULATIONS

In this section, we briefly discuss the simulation data as well as the procedure that we use to construct our various data sets. The

two simulations we describe are part of the Symphony suite of cosmological zoom-in simulations (Nadler et al. 2023). We refer the reader to Nadler et al. (2023) for a more detailed description of the simulations. The technique that we use for extracting data sets of host haloes and subhaloes is the same as that used in both Mezini et al. (2023) and Fielder et al. (2020). We refer the reader to these earlier works for more detailed descriptions of this procedure.

2.1 Milky Way and cluster mass zoom-in simulations

We use two sets of zoom-in cosmological simulations from the Symphony suite, each representing a different halo mass range. The first set of simulations, which were first presented in Mao, Williamson & Wechsler (2015), contains high-resolution zoom-in simulations of 45 Milky Way-mass haloes with particle mass $4.0 \times 10^5\,\mathrm{M}_\odot$ from a c125-2048 parent box run with L-GADGET (see Becker 2015). Halo masses in this catalogue are $M_{\rm vir} = 10^{12.09\pm0.02}\,\mathrm{M}_\odot$. The host haloes in this catalogue have between 83 ± 18 subhaloes at $z = 0$, where the quoted range corresponds to the 1σ host-to-host scatter in the number of subhaloes. The second set contains zoom-in simulations of 96 cluster-mass haloes with particle mass $1.8 \times 10^8\,\mathrm{M}_\odot$ that are within the mass range $10^{14.96\pm0.03}\,\mathrm{M}_\odot$ first presented in Wu et al. (2013). The host haloes in this catalogue have 210 ± 31 subhaloes at $z = 0$. We exclude one halo from the cluster-mass set due to a potential mislabelling between host halo and most massive subhalo.

2.2 Halo identification

Dark matter haloes in these simulations were identified by the *ROCKSTAR* (version 0.99.9-RC3+) halo finder (Behroozi, Wechsler & Wu 2013). In summary, *ROCKSTAR* is a 6D phase-space-based finder that produces catalogues of all the haloes identified as well as tables of all the particles associated with each halo. A more detailed description of *ROCKSTAR* can be found in Behroozi et al. (2013); the source code is publicly available.[1] We use the tables of particles which are produced for each halo to analyse subhalo positions and angular momenta relative to that of their hosts.

Our *ROCKSTAR* based definition of halo components is the same as in the previous works of Fielder et al. (2020) and Mezini et al. (2023) and translates into the following three groupings of halo particles.

(i) *host only*: These are particles that are associated with the host halo but *not* associated with any subhaloes identified by *ROCKSTAR*. The *host only* particles are part of the smooth component of the host halo or diffuse structures such as streams that are not identified by *ROCKSTAR*.

(ii) *subhalo only*: These are particles associated with at least one subhalo within the host halo, as identified by *ROCKSTAR*. Subhaloes within the Symphony simulation are defined such that they contain a minimum of 300 particles at $z = 0$.

(iii) *total halo*: These are particles associated with the host halo, including all particles associated with subhaloes within the host. In the vast majority of analyses in the literature, this is the set of particles that is used to characterize a halo; however, both Fielder et al. (2020) and Mezini et al. (2023) have found that the smooth, *host only* component of the host halo is markedly different from the *total halo* particles in a number of important ways.

[1] https://bitbucket.org/gfcstanford/rockstar

From the preceding definitions, it follows that combining the particles in the *host only* and *subhalo only* samples recover the set of particles in the *total halo* particle set.

3 QUANTIFYING HALO SHAPE AND ORIENTATION

3.1 The major axis of the host halo

The shapes of dark matter haloes are most often characterized by the ratios of the lengths of their principle axes. We will refer to the principle semi-axes lengths as a, b, and c, so that $a > b > c$. The major axis length is thus a. Dark matter haloes are most often found to be nearly prolate ellipsoids, which have $a > b \sim c$, but they can also be triaxial ellipsoids where $a > b > c$, and b and c are significantly different from one another.

The lengths of the principle axes can be computed as the eigenvalues of the inertia tensor, while their orientations are specified by the eigenvectors. The largest eigenvalue specifies a, while the smallest eigenvalue is c. The inertia tensor is

$$I_{ij} = \sum_n x_{i,n} x_{j,n}, \tag{1}$$

where $x_{i,n}$ and $x_{j,n}$ are the coordinates of the nth particle and the sum is over all particles identified with a halo. All particles in our simulations have identical masses, so there is no need to include the particle masses in the sum above.

In Fig. 1, we show the distribution in halo shapes within the Milky Way-mass and cluster-mass simulations. In both figures, the filled histogram corresponds to the ratio between the minor and major axes (c/a) and the hollow histogram to the ratio between the semimajor and major axis (b/a). For both c/a and b/a, cluster-mass haloes tend to be less spherical compared to Milky Way-mass haloes. Milky Way-mass haloes have a median c/a value of 0.74 ± 0.11 and b/a of 0.85 ± 0.10. For cluster-mass haloes, these values are 0.67 ± 0.08 and 0.77 ± 0.1, respectively. We additionally consider the relationship between halo shape and the proportion of host halo mass locked up in subhaloes. For both mass groups, we calculate the fraction of mass in subhaloes for each host and split the host haloes into 50th percentile groupings based on the fraction of mass in subhaloes. We find that the median c/a value is smaller (i.e. haloes are more elliptical) for host haloes in the group with high subhalo mass fractions; however, the difference is not statistically significant. For Milky Way-mass haloes, the low subhalo mass median shape is 0.78 ± 0.11 and the high subhalo mass median shape is 0.69 ± 0.10. For cluster-mass haloes, these values are 0.69 ± 0.07 and 0.66 ± 0.08.

We find the directions of the principle axes of the halo by calculating the inertia tensor and its eigenvectors directly from the particle data. We find the inertia tensor for the *subhalo only* component of each halo by subtracting the inertia tensor of the *host only* component from that of the *total halo* set. We then diagonalize this inertia tensor to get the subhalo component principle axes.

3.2 Halo and subhalo angular momentum

Similar to the major axis, angular momentum is also calculated directly from particle data. Per particle, we calculate the cross product of $\boldsymbol{r}_n$, the position of the nth particle with respect to the host halo's centre, and $\boldsymbol{v}_n$, the velocity of nth particle, also with respect to the host halo centre. Summing over the angular momenta of all particles

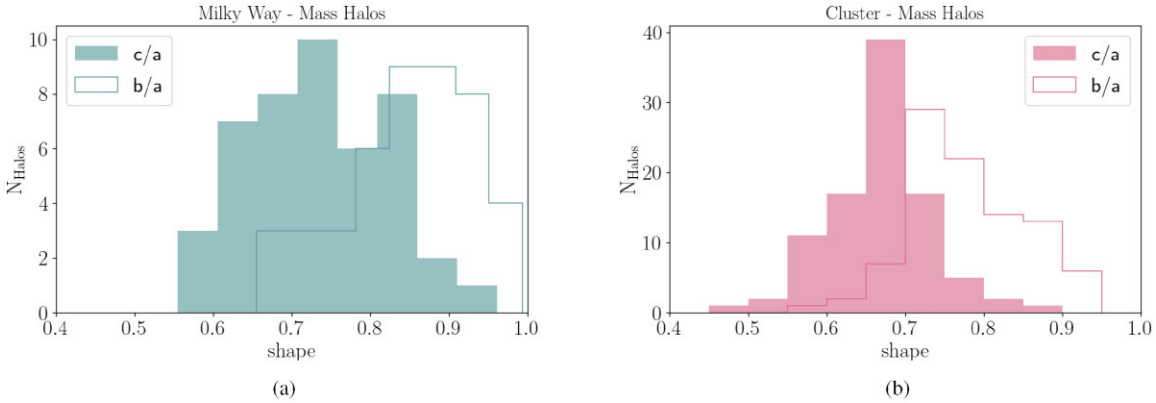

Figure 1. Distributions of halo shape as measured by the ratio of the halo minor axis to major axis (c/a) and the semimajor to major axis (b/a). The filled histograms correspond to c/a and hollow histograms to b/a. Milky Way-mass haloes are shown in panel (a) on the left and cluster-mass haloes on right in panel (b). Cluster-mass haloes are generally less spherical.

gives the total halo angular momentum,

$$\boldsymbol{J} = \sum_n m_n(\boldsymbol{r}_n \times \boldsymbol{v}_n), \tag{2}$$

where m_n is the mass of the nth particle. The total angular momentum, $\boldsymbol{J}_{\rm Tot}$, includes the angular momentum associated with both host halo and subhalo particles and is computed by summing over the *total halo* particle set. The host angular momentum, $\boldsymbol{J}_{\rm Host}$, is calculated using equation (2) by summing over the *host only* particle set, while the angular momentum carried by the subhaloes, $\boldsymbol{J}_{\rm Sub}$, is defined to be the difference $\boldsymbol{J}_{\rm Sub} = \boldsymbol{J}_{\rm Tot} - \boldsymbol{J}_{\rm Host}$.

3.3 The subhalo mass distribution

We are interested in the way in which the substructure of a halo is distributed about its host. The distribution of subhaloes around their hosts in two-dimensional projection and whether this distribution varies based on the projection angle are of special interest due to their relevance to gravitational lensing. Two-dimensional projections are an interesting special case because the projected 2D density is the relevant quantity in lensing which results in the angular deflections that distort the source. A number of strong lensing analysis programs count among their goals to infer the properties of subhaloes (and other line-of-sight haloes) in projection (e.g. Oguri & Marshall 2010; Mckean et al. 2015; Ivezic et al. 2019). To this end, we calculate the projected mass in subhaloes near the halo centre from different viewing angles, including projections along the major axis, for which the projected mass density is highest. We recommend referring to Fig. 2 while reading the steps of this calculation. Our procedure is as follows.

(i) Define a set of axes along which to project host halo and subhalo mass. The axes are centred on the host halo and spaced isotropically over the surface of a sphere.

(ii) Define a cylinder, with a central axis that points along the halo major axis and intersects the halo centre such that the circular face of the cylinder has a radius $r < r_{\rm VIR}$ and the length of the cylinder extends to the virial radius of the halo.

(iii) Measure the total mass of subhalo particles that fall within the cylinder and divide it by the total halo mass to calculate the subhalo mass fraction within the cylinder.

(iv) Rotate the cylinder about the halo centre so that it points along the subsequent axis in the predefined set of projection axes.

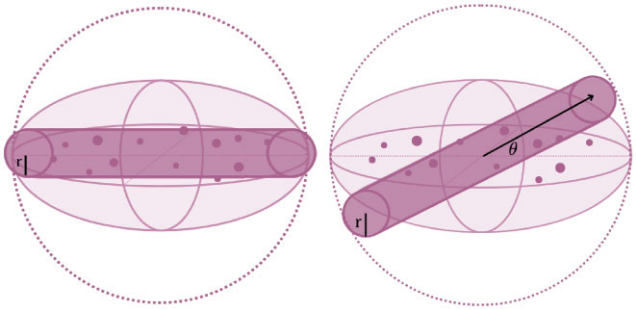

Figure 2. Diagram showing how cylinders are defined to calculate projected mass as described in Section 3.3. The dotted circle represents the region enclosed within the virial radius of the halo. The light shaded ellipsoid represents the shape of the host halo even though all particles within the virial radius are used, and the filled in dark circles represent subhaloes. The left image shows a cylinder of radius r oriented near the major axis. The cylinder is then rotated to some random orientation as shown in the right image. When comparing the left and right images, we can see how the number of subhaloes within cylinders of the same size can vary depending on orientation.

(v) Calculate the angular separation, θ, between the major axis and the new axis of projection.

(vi) Repeat the mass measurement from step (iii).

(vii) Repeat the process of rotating and measuring the subhalo mass [steps (iii)–(vi)] within each rotated cylinder for all the axes in the predefined set of axis directions from step (i).

This procedure is repeated for each halo of the Milky Way-mass and cluster-mass haloes separately for cylinders with logorithmically spaced radii from 0.001 to 1 times their host virial radius. By definition, a radius of $r = 0$ encompasses none of the halo mass, whereas a cylinder of radius $r = r_{\rm VIR}$ encompasses the entire halo. Once completed, for both cluster-mass and Milky Way-mass haloes, we will have a distribution of subhalo mass fractions within a cylinder of radius r as a function of the angle θ between the cylinder's axis and the halo's major axis.

4 RESULTS I: HOST HALO ALIGNMENTS

We begin our discussion of halo alignments with a study of the properties of particles that are associated with the host halo. It has been found that the orientation of the halo angular momentum vector

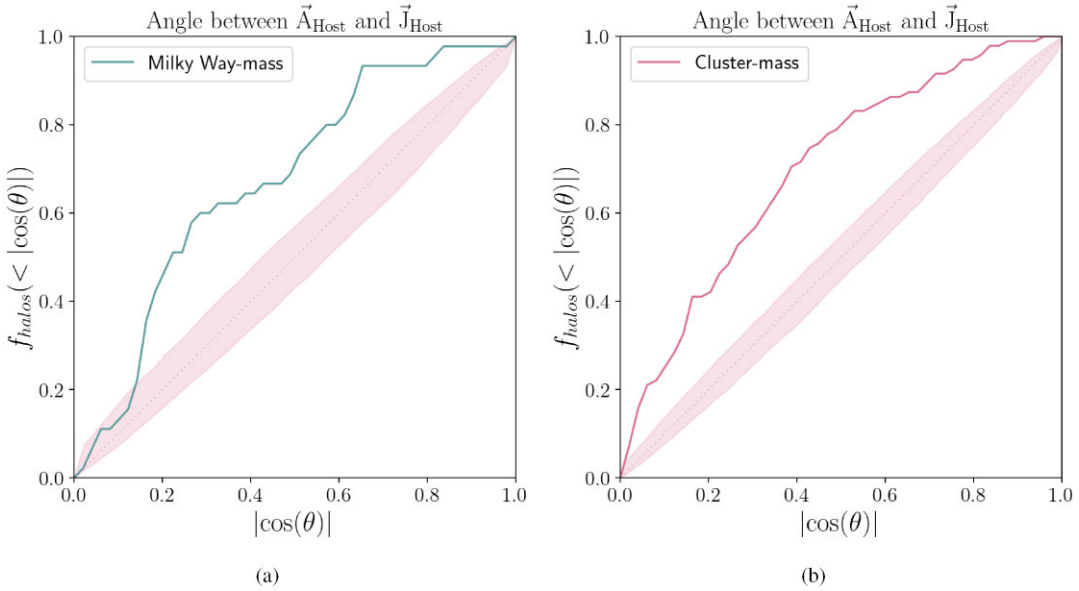

Figure 3. The cumulative fraction of haloes with angle less than $\cos(\theta)$ between the host halo angular momentum vector, $\boldsymbol{J}_{\rm Host}$ and its major axis $\boldsymbol{A}_{\rm Host}$ as a function of $\cos(\theta)$. The solid line is the result from the simulation data, the dashed line and the filled area are the cumulative distribution function (CDF) for an isotropic distribution and the area within the 14th and 86th percentiles. The percentiles are computed from random samples that are the same size as the simulation samples. Results for Milky Way-mass haloes are shown in (a) and cluster-mass in (b).

with respect to the principle axes of the halo is not isotropic. Rather, the angular momentum vector is correlated with the minor axis of the halo (e.g. Warren et al. 1992; Tormen 1997), as expected from tidal torque theory (e.g. Porciani, Dekel & Hoffman 2002a, b). The halo major and minor axes are orthogonal to one another (by definition). Therefore, this suggests that the angular momentum of a halo should be oriented in a manner that is preferentially orthogonal to its major axis.

In Fig. 3, we show the cumulative probability distribution of haloes as a function of the cosine of the angular separation, $|\cos(\theta)|$, where θ is the angle between the host halo angular momentum vector, $\boldsymbol{J}_{\rm Host}$, and the host major axis. The angle θ plays the role of a zenith angle with zero along the angular momentum vector, so a model in which angular momenta and major axes are uncorrelated would yield a uniform distribution of $|\cos(\theta)|$. Panel (a) corresponds to Milky Way-mass haloes and (b) to cluster-mass. In each panel, the solid lines represent the cumulative distribution function of alignments from our simulation data sets. The straight dotted lines represent the distribution expected for a random, isotropic relation between angular momentum and major axis. The filled areas represent errors relative to an isotropic underlying true distribution. These errors were estimated by building 1000 mock samples of alignments from an isotropic underlying distribution. Each mock sample contained the same number of data points as the simulation data (45 for Milky Way mass and 95 for cluster mass). The errors are then the 16th and 84th percentiles of these mock samples.

As discussed above, we expect that the orientation of $\boldsymbol{J}_{\rm Host}$ with respect to host halo major axes is not isotropic and will be preferentially aligned with the minor axes, and perpendicular to the major axes. Our data are suggestive of an orthogonal alignment between the major axis and angular momentum vector, $\boldsymbol{J}_{\rm Host}$, as expected. In both panels of Fig. 3, we see an excess of haloes for which the angle between the angular momentum vector and the major axis, $|\cos(\theta)|$, is small, which corresponds to a perpendicular alignment. The Kolmogorov–Smirnov (KS) probability that these angular distributions are selected from an isotropic distribution is $\sim 4 \times 10^{-5}$ for Milky Way-mass haloes and $\sim 3 \times 10^{-5}$ for cluster-mass haloes, indicating that an isotropic, uncorrelated distribution of halo angular momenta and principle axes is excluded by the data. This alignment has previously been detected in works such as Shaw et al. (2006), Knebe et al. (2008), Deason et al. (2011), Hoffmann et al. (2014), and Kiessling et al. (2015).

We can also quantify the alignment between host halo angular momentum vector and host major axis with the median angular separation between the two. For Milky Way-mass haloes, the median angular separation is $\theta = 77 \pm 3.0^\circ$ (17°) or $|\cos(\theta)| = 0.22 \pm 0.05$ (0.24). The first set of error values are the errors on the medians while the values in the parentheses correspond to the dispersions in the distribution of angles. For cluster-mass haloes, the median angular separation is $\theta = 75 \pm 2^\circ$ (16°) or $\cos(\theta) = 0.25 \pm 0.04$ (0.24). Errors are calculated by bootstrapping. For each set of angles, we sample the angles with replacement to create a mock sample of the same size and calculate its median. To get the uncertainty we repeat this 1000 times and calculate the standard deviation of the set of 1000 medians. For an isotropic distribution of angles, we would expect a median of 60°, however, we are measuring angles that are approximately 15° greater. Angles significantly greater than 60° are indicative of perpendicular alignment which is consistent with the discussion in the previous paragraph that a halo's angular momentum vector is preferentially perpendicular to its major axis.

5 RESULTS II: SPATIAL DISTRIBUTION OF SUBHALOES

Next, we study the spatial distribution of subhaloes about their hosts in two ways. First, we measure the degree to which the spatial positions of subhaloes are aligned with the major axis of their host halo and whether or not subhaloes reside in a planar structure roughly orthogonal to the host angular momentum. Secondly, we measure the way in which the 2D projection of the subhalo population belonging

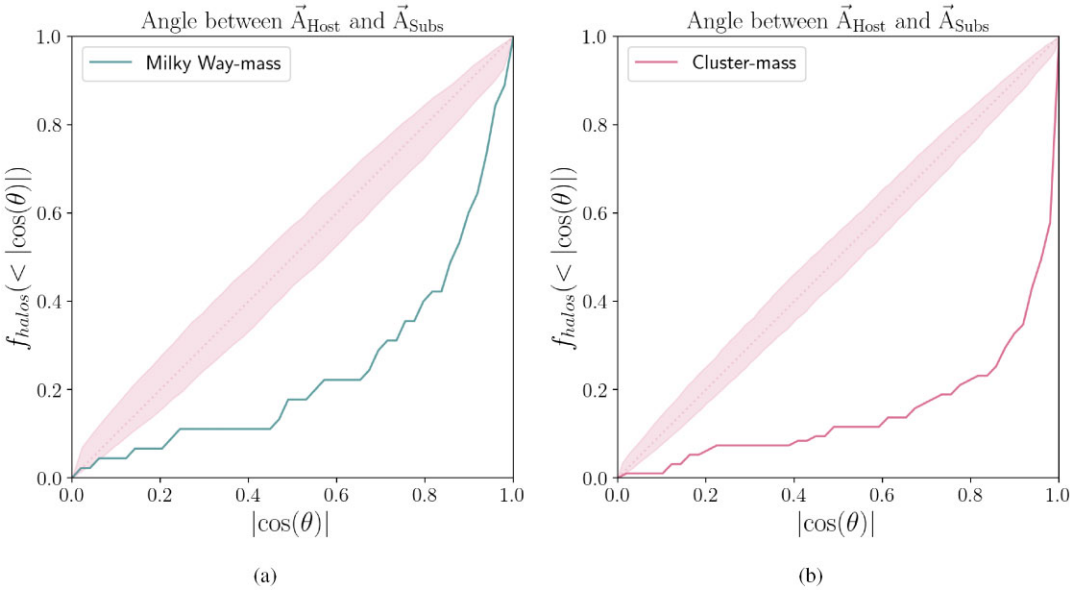

Figure 4. The cumulative fraction of haloes with angle $<|\cos(\theta)|$ between the host halo major axis $\boldsymbol{A}_{\rm Host}$ and that of its subhaloes, $\boldsymbol{A}_{\rm Sub}$, as a function of $|\cos(\theta)|$. The solid line is the result from the simulation data, the dashed line and the filled area are the cumulative distribution function (CDF) for an isotropic distribution and the area within the 14th and 86th percentiles. Panel (a) is for Milky Way mass haloes and (b) is for cluster-mass haloes.

to a host changes when the halo is viewed from different directions. We quantify this projection effect primarily in terms of the projected mass fraction in subhaloes.

5.1 Principle axis and angular momentum alignments of subhaloes and their hosts

We first discuss alignments between the major axis of the distribution of all subhaloes belonging to a particular host halo and the major axis of said host halo. The principal axes of the subhalo component are defined as the eigenvectors of the inertia tensor corresponding to subhalo particles only. We calculated the angular separation between the major axis of the host, $\boldsymbol{A}_{\rm Host}$, and that of the subhaloes, $\boldsymbol{A}_{\rm Sub}$. Previous works have shown that this result can vary as a function of the radius at which the calculation is performed (Schneider, Frenk & Cole 2012). In this work, we chose to use major axis as defined up to the full virial radius of the halo. In Fig. 4, we show the cumulative fraction of haloes with angle $< |\cos(\theta)|$ between $\boldsymbol{A}_{\rm Host}$ and $\boldsymbol{A}_{\rm Sub}$ as a function of $|\cos(\theta)|$. The left plot (Fig. 4a) shows results for Milky Way-mass haloes and the right (Fig. 4b) for cluster-mass haloes.

In both panels of Fig. 4, we see that there is a deficit of haloes at smaller values of $|\cos(\theta)|$, indicating that the angular separation between the major axis of the host halo matter distribution and the major axis of the subhalo distribution is smaller than it would be given an isotropic distribution. This implies, perhaps unsurprisingly, that $\boldsymbol{A}_{\rm Host}$ and $\boldsymbol{A}_{\rm Sub}$ are preferentially aligned. In other words, the distribution of subhaloes is aligned with the distribution of host halo mass. The KS probability that the result for Milky Way-mass haloes (Fig. 4a) is selected from an isotropic distribution is $P_{\rm KS}$ is $\sim 3 \times 10^{-9}$. For cluster-mass haloes (Fig. 4b) this probability is $\sim 7 \times 10^{-10}$.

For Milky Way-mass haloes, the median angle between the host halo major axis the subhalo component major axis is $\theta = 30 \pm 4.0^\circ$ (22°) or $|\cos(\theta)| = 0.86 \pm 0.04$ (0.26). For cluster-mass haloes, this median angle is $\theta = 16 \pm 3^\circ$ (23°) or $|\cos(\theta)| = 0.96 \pm 0.01$ (0.24). Errors are calculated with the same bootstrap method as Section 4. For an isotropic distribution of angles (spanning from 0° to 90°), we would expect a median of 60°; however, we measure angular separations that are approximately 30°–45° smaller. This is consistent with the discussion in the previous paragraph that subhaloes preferentially reside closer to the major axis of their host halo.

The alignment we find between $\boldsymbol{A}_{\rm Host}$ and $\boldsymbol{A}_{\rm Sub}$ is not unexpected, a fact to which we have already alluded. Within the model of hierarchical structure growth, subhaloes merge with host haloes in a correlated manner along filaments (e.g. Jing & Suto 2002; Plionis & Basilakos 2002; Bailin & Steinmetz 2005; Faltenbacher et al. 2005; Zentner et al. 2005b; Shaw et al. 2006; Libeskind et al. 2007; Welker et al. 2014). In a recent work, Han et al. (2023) showed that $\sim$ 68 per cent of accreted subhaloes enter their host halo through $\sim$ 38 per cent of the halo surface area defined at the virial radius. This results in alignment between the large-scale filamentary structure and that of a host halo (e.g. Jing & Suto 2002; Bailin & Steinmetz 2005; Faltenbacher et al. 2005; Zentner et al. 2005b). In turn, this causes the shape and orientation of haloes to be ellipsoids with their longest axes pointed along the direction of the filament. Consequently, subhaloes are preferentially located near this longest axis, the major axis, and this is the alignment that we detect.

Comparing Fig. 4(a) with Fig. 4(b), it is evident that the alignment between $\boldsymbol{A}_{\rm Host}$ and $\boldsymbol{A}_{\rm Sub}$ is more pronounced in cluster-mass haloes than in Milky Way-mass haloes. This difference may be attributed to the later formation times and larger subhalo abundances of cluster-mass haloes, which generally have experienced significantly more recent mergers (Lacey & Cole 1994; Wechsler et al. 2002; Zentner et al. 2005a). Consequently, this means that the major axes of cluster-mass haloes have been more recently influenced by the influx of mergers along neighbouring filaments. Collectively, these effects lead to subhaloes being positioned more closely to the major axis of cluster-mass haloes. Such a mass dependence on the strength of alignments has been proposed before for neighbouring haloes in works such as Jing (2002), Schneider et al. (2012), Li et al. (2013), and Xia et al. (2017). A follow-up analysis would be necessary in order to confirm this interpretation.

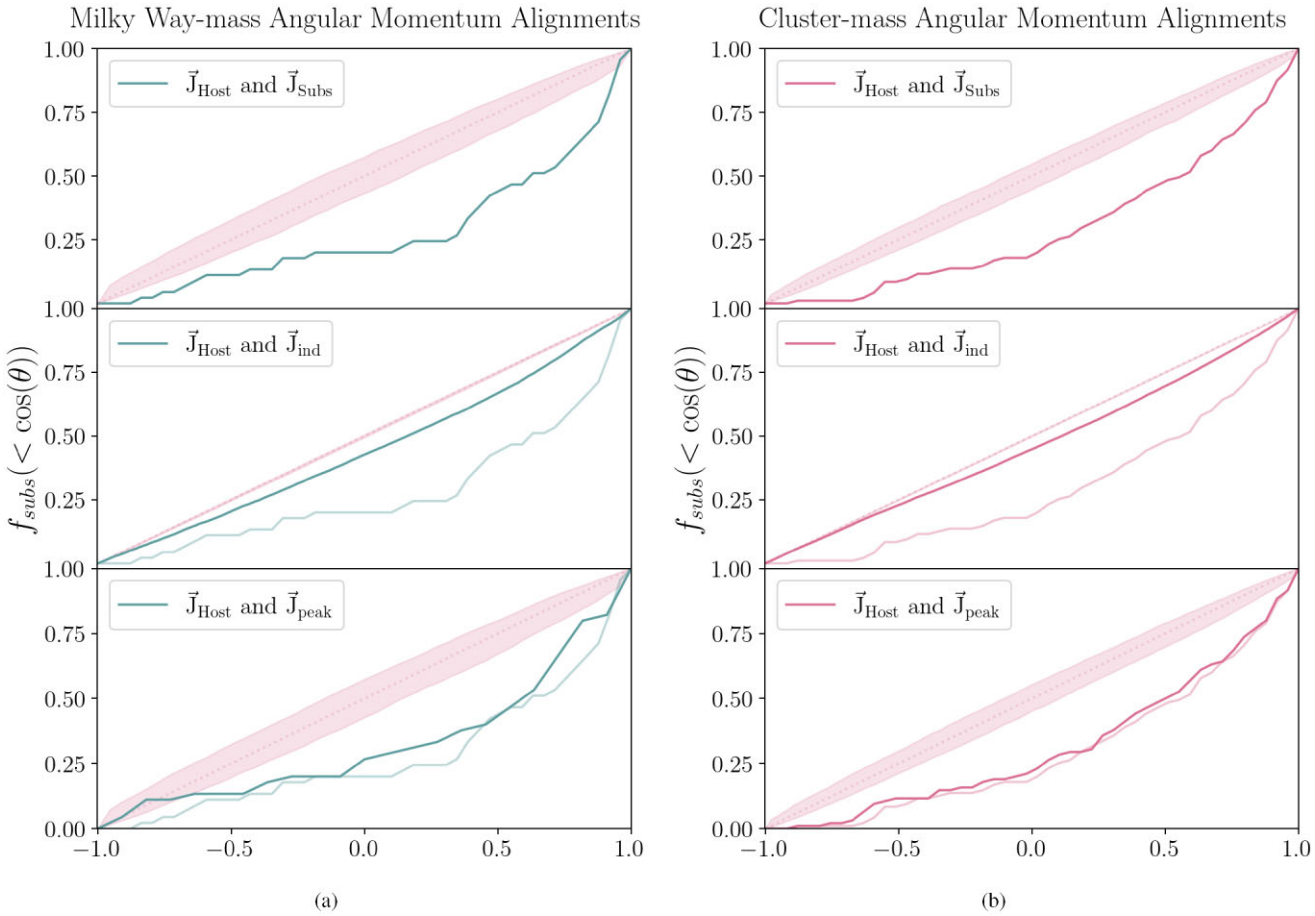

Figure 5. The same as Fig. 4 except for the angles between the host and subhalo angular momentum vectors, $\boldsymbol{J}_{\rm Host}$ and $\boldsymbol{J}_{\rm Sub}$, respectively. In the bottom four figures, we use alternative measurements of subhalo angular momentum. For comparison with the original method of measuring subhalo angular momentum, we also plot the lines from the top plots in a lighter shade along side the alternative method result. In the middle row, subhalo angular momenta is defined by the position and velocity of its density peak. Like in the top row figures, we sum over all subhalo angular momenta to define $\boldsymbol{J}_{\rm peak}$. In the bottom row, $\boldsymbol{J}_{\rm ind}$ corresponds to the angular momentum of a single subhalo found by summing over all its particles rather than the sum of particles over all subhaloes belonging to a host.

In principle, it may be possible for the major axes of host halo and subhalo components to be aligned without an anisotropic distribution of subhaloes (though this seems inconsistent with our other results, see below). Suppose that the distribution of subhaloes is characterized by principle axial ratios $(b/a)_{\rm subs}$ and $(c/a)_{\rm subs}$ (from the *subhalo only* samples) that are significantly larger than the principle axial ratios determined by the overall mass of the host haloes (from the *host only*) samples. For example, if $(c/a)_{\rm subs} \sim 1 \gg (c/a)$ and $(b/a)_{\rm subs} \sim 1 \gg (b/a)$, then the subhalo mass would be distributed nearly isotropically, so that axis alignments would be far less noteworthy. However, this is not the case. We find that subhalo mass is distributed approximately as anisotropically as its host halo's mass as quantified by axial ratios. The axial ratios for host haloes in the Milky Way-mass simulations are $(b/a) = 0.86 \pm 0.10$ and $(c/a) = 0.74 \pm 0.11$, while the corresponding ratios for subhalo mass are $(b/a)_{\rm subs} = 0.84 \pm 0.16$ and $(c/a)_{\rm subs} = 0.66 \pm 0.16$. Similarly, for cluster-mass haloes the axial ratios are $(b/a) = 0.78 \pm 0.08$ and $(c/a) = 0.68 \pm 0.07$ for host haloes while they are $(b/a)_{\rm subs} = 0.60 \pm 0.2$ and $(c/a)_{\rm subs} = 0.36 \pm 0.18$ for the subhaloes. Subhalo mass is distributed at least as anisotropically as the host halo mass indicating that alignments among principle axes designate meaningful alignments of a strongly anisotropic distribution of subhaloes. In fact, our results suggest that the distribution of subhalo mass is somewhat less spherical than the overall mass distribution of a halo.

In Fig. 5, we compare the angular momentum vectors of host haloes, $\boldsymbol{J}_{\rm Host}$, to that of their subhaloes, $\boldsymbol{J}_{\rm Sub}$. $\boldsymbol{J}_{\rm Host}$, and $\boldsymbol{J}_{\rm Sub}$ are both defined in Section 3.2. Notice that, unlike orientations relative to the major axis, the x-axis in Fig. 5 is $\cos(\theta)$ rather than $|\cos(\theta)|$ to display cases in which subhalo angular momenta are anti-parallel to that of their host. The left panels correspond to Milky Way-mass haloes and the right to cluster-mass haloes. In the top row, figures *a* and *b*, we see a similar trend as in Fig. 4 in which there is a deficit of haloes at smaller values of $\cos(\theta)$, indicating that there is alignment between $\boldsymbol{J}_{\rm Host}$ and $\boldsymbol{J}_{\rm Sub}$. The KS probability that the distribution for Milky Way-mass haloes in the top panel of Fig. 5(a) is selected from an isotropic distribution is $P_{\rm KS} \sim 1 \times 10^{-9}$. For cluster-mass haloes in the top panel of Fig. 5(b), $P_{\rm KS}$ is $\sim 4 \times 10^{-5}$. As we discussed in the preceding paragraph, the tendency for subhalo and host halo angular momenta to be aligned makes sense within the context of hierarchical growth – subhaloes merging in from coherent directions along filaments will preferentially orbit near a plane containing the major axis. The fact that we detect alignment between major axes strengthens this argument.

The other two rows of panels in Fig. 5 show our results for alternative methods of measuring the subhalo angular momentum. In

the first case, we define the angular momentum of each subhalo using the position and velocity of its centre as specified in the halo catalogue and sum over that angular momentum for all subhaloes within a host to find the total angular momenta of the subhalo component of the halo. We will refer to this measure of angular momentum as $\boldsymbol{J}_{\rm peak}$. This method is distinct from the previous method in which the subhalo angular momenta were computed by summing over the particle content of each subhalo. In panels *c* and *d* we show the cumulative distribution of angles between $\boldsymbol{J}_{\rm peak}$ and $\boldsymbol{J}_{\rm Host}$. The distributions in *c* and *d* are, unsurprisingly, both similar to those of *a* and *b*. This suggests that our alignment results are insensitive to the details of the method used to determine subhalo angular momenta. In the second alternative case, we display the alignments of angular momenta for *individual* subhaloes, rather than for populations of subhaloes associated with individual hosts. In particular, we compute the angle between the angular momentum of each individual subhalo and the angular momentum vector of its host. To distinguish this measurement, we refer to the angular momentum of a single subhalo as $\boldsymbol{J}_{\rm ind}$. We sum over the angular momenta of all particles in any individual subhalo to determine $\boldsymbol{J}_{\rm ind}$. The result of this exercise is shown in the bottom panels, *e* and *f*. The resulting distribution of alignments differs from those in panels *a*, *b*, *c*, and *d*, because in this case the individual subhaloes corresponding to a single host can fall into distinct bins of zenith angle, whereas in the previous calculation each host had a single zenith angle corresponding to the alignment of the host angular momentum with the net angular momentum of the population of subhaloes. This has the effect of spreading the contribution from the subhalo population associated with any particular host galaxy among a range of zenith angle values. Furthermore, the alignment distribution computed in this way is significantly less noisy because the distribution is assembled from many more data points. Calculating angles for individual haloes allows us to decipher whether or not the alignment in the top two figures, *a* and *b*, is due to a large fraction of subhaloes having angular momenta aligned with that of their hosts, or, subhalo angular momenta that are spread out but average to a value close to that of its host. The anisotropy is weaker for $\boldsymbol{J}_{\rm ind}$, implying that those subhaloes with the largest angular momenta are more well-aligned with the host angular momentum.

Finally, we quantify the alignment between angular momenta with the median angular separation between host and subhalo angular momentum vectors. For Milky Way-mass haloes, the median angular separation is $\theta = 50 \pm 9^{\circ}(38.0^{\circ})$ or $\cos(\theta) = 0.63 \pm 0.12$ (0.55). For cluster-mass haloes, it is $\theta = 56 \pm 5.5^{\circ}(34^{\circ})$ or $\cos(\theta) = 0.56 \pm 0.08$ (0.49). Errors are calculated by bootstrapping using the same method as in Section 4. For an isotropic distribution of angles (spanning from 0° to 180°), we would expect a median of 90°, with 0° indicative of perfect alignment between the angular momentum vectors, and 180° indicative of $\boldsymbol{J}_{\rm Host}$ and $\boldsymbol{J}_{\rm Sub}$ pointing in complete opposite directions. Our findings show that the median angle of separation between angular momentum of the host and subhaloes is significantly smaller than 90°, indicative of strong alignment between the two, and is consistent with the discussion in the previous paragraph that subhaloes should orbit in the same plane as the host halo.

Although we anticipate that the alignments of $\boldsymbol{A}_{\rm Sub}$ and $\boldsymbol{A}_{\rm Host}$, and, $\boldsymbol{J}_{\rm Sub}$ and $\boldsymbol{J}_{\rm Host}$ are a result of mergers along coherent directions, such as filaments, we should expect significant scatter in these alignments. Cluster-sized haloes are comparable in size to the filament in which they reside and may also be located at a node connecting multiple filaments. Galaxy-sized haloes at present are often smaller than the size of the filaments in which they live but may have accreted their surviving subhaloes at times when filaments were thinner (Vera-Ciro et al. 2011). The distribution of subhaloes that merge from other directions or from presently subdominant filamentary structure introduces considerable scatter into the anisotropic distributions we have found. Furthermore, simulations have shown that spin alignment with filaments has a mass dependence (Bailin & Steinmetz 2005; Aragón-Calvo et al. 2007; Paz, Stasyszyn & Padilla 2008; Zhang et al. 2009; Libeskind et al. 2010; Codis et al. 2012; Forero-Romero, Contreras & Padilla 2014; Libeskind et al. 2015). In particular, Codis et al. (2012) find that the orientation of a halo's spin relative to the filament in which it resides has a mass dependence with a turnover from pointing parallel to the filament to perpendicular at a critical mass of $\sim 5\ (\pm 1) \times 10^{12}\,{\rm M}_{\odot}$. This mass is greater than that of our Milky way-mass haloes and considerably lower than that of our cluster-mass haloes. This suggests that Milky Way-mass haloes will be oriented differently relative to the present-day large-scale structure than cluster-mass haloes will. This is interesting to note and may be important for a variety of forthcoming applications, including gravitational lensing studies, but we will not pursue this further in this work.

5.2 The distribution of subhalo mass as a function of viewing angle

In order to interpret strong gravitational lensing measurements, it is most practical to focus on the mass in the central region of the halo and specifically, the mass within approximately the Einstein radius in projection. For lenses at $z = 0.5$ composed of a galaxy within a dark matter halo within the mass range of our Milky Way-mass haloes, with a source at $z = 2$, we estimate an Einstein radius of approximately 2 arcsecs or 12.2 kpc and for lenses composed of a galaxy in a cluster-mass dark matter halo they are approximately 10 arcsecs or 61 kpc. Because of the ellipsoidal shape of haloes, the projected matter density near the centre will vary depending on the orientation from which the halo is viewed and a greater projected matter density will be observed near the centre when the halo is viewed along its long axis compared to its shortest. We predict that a greater projected density of subhaloes at the halo centre will also be observed when the halo is viewed along this axis.

Determining the influence of subhaloes on strong lensing systems is a topic of great contemporary interest. We have already demonstrated that subhaloes are distributed anisotropically around their hosts and that subhaloes are found preferentially aligned the long axes of their hosts. We quantify this effect to inform its importance in previous and forthcoming lensing measurements. We show the results from this analysis in Fig. 6 where the left panels correspond to Milky Way-mass haloes and the right panels to cluster-mass haloes. The panels of Fig. 6 depict the mass fraction in subhaloes in a cylindrical projection as a function of both radius of the cylindrical projection (top panels) and viewing angle relative to the major axis of the halo (bottom panels). The cylinder scheme was discussed in Section 3 and it may be useful to review Fig. 2 to visualize the geometry under consideration. In all panels, the vertical axis is the ratio of the projected subhalo mass fraction enclosed within a particular cylinder, oriented at an angle θ away from the halo major axis, divided by the median mass fraction for all cylindrical projections across all haloes and angles.

In the top two panels of Fig. 6, the solid line is the median normalized subhalo mass fraction within bins of $r/r_{\rm VIR}$ at four different angular separations ranging from aligned with the major axis (lightest shaded line) to perpendicular to the major axis (darkest shaded line). The shaded regions are the error margins corresponding to 14th and 86th percentiles. Mass fractions are normalized by

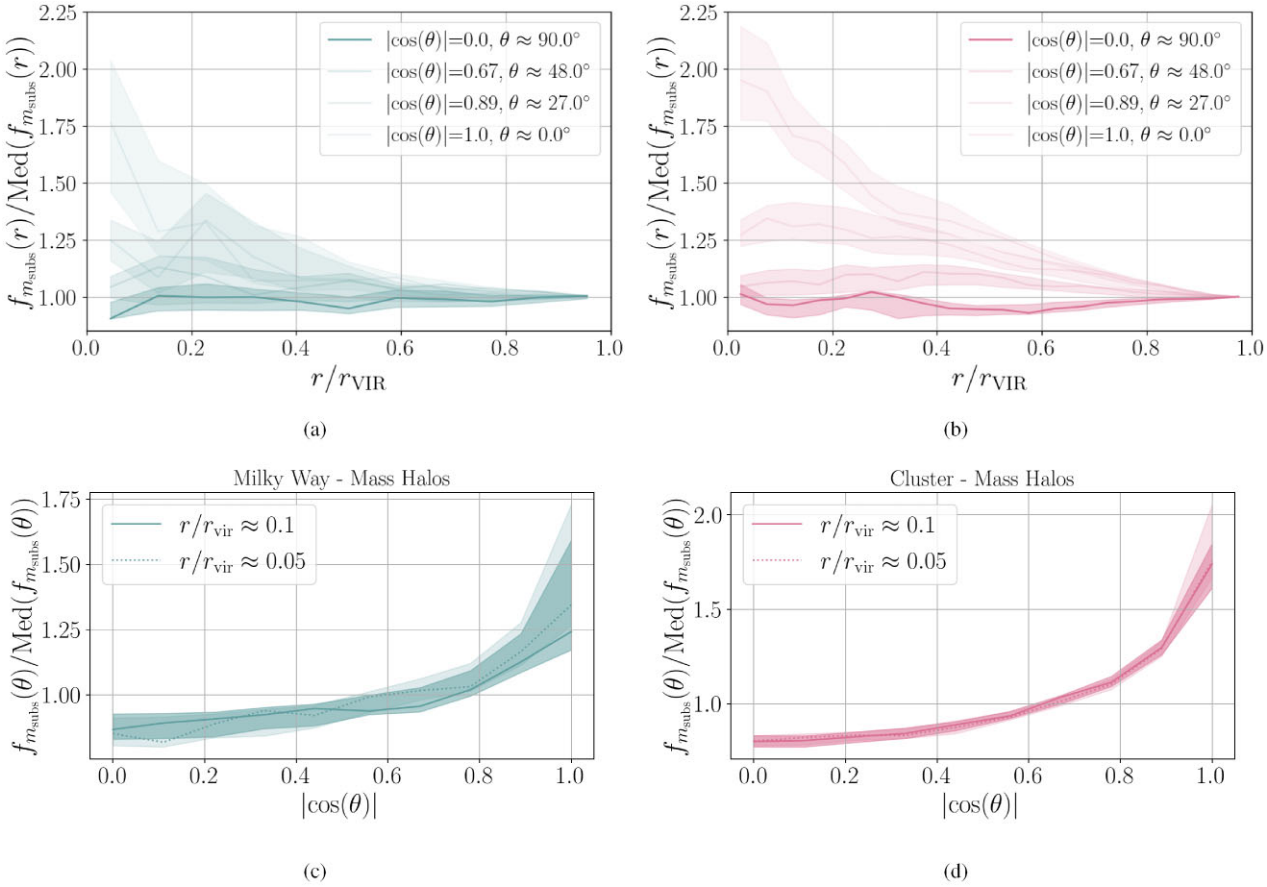

Figure 6. The top two panels show subhalo mass fraction captured within cylinders projected along predefined axes on a uniformly spaced grid on the surface of a sphere normalized by the median mass fraction across all haloes and angles. The left panel corresponds to Milky Way-mass haloes and the right panel to cluster-mass haloes. The x-axis is the ratio of the radius of the cylinder to virial radius of the halo, and, the y-axis is the normalized subhalo mass fraction. The solid lines are the median normalized mass fraction within bins of $r/r_{\rm VIR}$ at four different angular separations ranging from aligned with the major axis (lightest shaded line) to perpendicular to the major axis (darkest shaded line). The bottom two panels contain the same information presented in a different way. For these figures, the x-axis is the angular separation. The solid and dotted lines correspond to the mass fraction within cylinders of radii equal to approximately 10 per cent and 5 per cent of the virial radius. The shaded regions are the error margins corresponding to 14th and 86th percentiles.

the median subhalo mass fraction across all haloes and angles. Consequently, if the subhaloes were distributed isotropically, the solid lines in each panel would be horizontal lines with a value of 1.0. In both Milky Way-mass and cluster-mass haloes, the subhalo mass fraction increases as cylinder orientation approaches the major axis. Smaller cylinder radii lead to dramatically larger differences, which makes sense because smaller cylinder radii correspond to averaging over a smaller physical scale so that correlations are not washed out by subhaloes that are poorly aligned with the major axis, but fall within the cylinder radius. This effect is more dramatic for cluster-mass haloes where the mass fraction is approximately 1.95 times greater at small cylinder radii along the major axis compared to perpendicular, whereas the trend for Milky Way-mass haloes is both smaller (1.75 times greater at small radii along the major axis) and noisier (due to the smaller sample size). The bottom two panels show the median normalized mass fraction within bins of separation angle at two cylinder radii equal to approximately 5 per cent and 10 per cent of the virial radius. Once again, the shaded regions are the bootstrapped error margins corresponding to 14th and 86th percentiles. In these figures, we again note an increase in mass fraction as cylinder orientation approaches the major axis for the same reason as discussed above. We note that the difference in maximum mass fraction between the top and bottom figures is due to the fact that in the bottom figures we are binning data in $\cos(\theta)$.

This result naturally emerges from the anisotropies already discussed in Section 5.1. We saw overall stronger alignments with particular axes for cluster-mass haloes in Section 5.1 as well, so the difference in the strength of this effect between Milky Way-mass haloes and cluster-mass haloes is not surprising. We attribute the noisiness in the Milky Way result to the fact that there are fewer than half as many Milky Way-mass host haloes compared to cluster-mass host haloes. Moreover, smaller host haloes tend to have a smaller total fraction of their mass in subhaloes, so the Milky Way-mass hosts contain fewer subhaloes and thus there is a larger shot noise associated with subhalo position.

For lensing, a massive subhalo of some mass, M, in the line of sight will leave a larger lensing signal than a collection of smaller subhaloes with collective mass, M. To this end, we ran a smaller scale version of the analysis discussed above with a variety of subsamples computed using threshold samples of subhaloes above a minimum mass. We calculate projected subhalo mass for subhaloes of mass, M, greater than 0.025, 0.05, 0.075, and 0.1 times the total halo virial mass. These numbers are selected such that they fall within

the range of available subhalo masses – Milky Way-mass haloes in our sample do not have subhaloes more massive than 0.2 times their total halo virial mass and only a handful of cluster-mass haloes have subhaloes that exceed this threshold. For this iteration of the analysis, we calculate the mass fraction at only two radii on the scale of the expected Einstein radius, 0.05 and 0.1 times the halo virial radius, along 500 randomly selected axes through the halo. We find that as this lower mass limit is increased, there is a small increase in the overabundance of projected subhalo mass near the major axis, although, the change is not statistically significant. When considered together with our other results indicating subhalo anisotropies, we nevertheless encourage the reader to be mindful of this potential effect.

6 CONCLUSION AND DISCUSSION

6.1 Conclusion

In this paper, we have shown that subhaloes are distributed anisotropically with respect to their host haloes. In particular, subhaloes tend to reside preferentially near the major axis of their host halo. We examined specifically the following relationships between the host halo and its subhalo population: (1) the degree to which the angular momentum of the host halo is correlated with the net angular momentum of its associated subhalo population; (2) the alignment of the principle axes of the host halo with the principle axes defined by its subhalo population; and (3) we measured the projected mass in subhaloes as a function of projection angle relative to the major axis of the host. This study anticipates applying these results to the interpretation of strong lensing observations, but we have phrased the alignment in a variety of ways so that these alignment results may be applied more broadly in a variety of other applications. To our knowledge, this is the only analysis of this type performed using zoom-in simulations of comparably high resolution. This has enabled us to study subhalo–host relationships in greater detail than previous studies. Our main results are as follows.

(i) Both cluster-mass and Milky Way-mass host halo's major axes are generally well aligned with those of their subhaloes. In this broad sense, subhaloes are preferentially oriented in the same way as the overall mass distribution of their host haloes. For Milky Way-mass haloes, the median angle between the host halo major axis the subhalo component major axis is $\theta = 30 \pm 4^\circ$ or $|\cos(\theta)| = 0.86 \pm 0.04$. For cluster-mass haloes, this median angle is $\theta = 25 \pm 3.5^\circ$ or $|\cos(\theta)| = 0.91 \pm 0.03$.

(ii) Both cluster-mass and Milky Way-mass host halo's angular momenta are fairly well aligned with the net angular momenta of their subhaloes. For Milky Way-mass haloes, the median angle between the host halo angular momentum the net subhalo angular momentum is $\theta = 50 \pm 9^\circ$ or $\cos(\theta) = 0.63 \pm 0.12$. For cluster-mass haloes, this median angle is $\theta = 56 \pm 5.5^\circ$ or $\cos(\theta) = 0.56 \pm 0.08$.

(iii) Haloes that are viewed along their major axis have a greater projected subhalo mass near their centres compared to those viewed along a random axis direction. As seen in the top panels of Fig. 6, within projected radii of a few per cent of the virial radius of the host halo, the fraction of mass in subhaloes is ~ 175 per cent larger for Milky Way mass haloes and as much as ~ 195 per cent larger for cluster haloes when projected along the major axis as compared to the average from a random projection. To within our ability to measure, this preference does not have a strong dependence upon the mass of the subhalo.

6.2 Discussion

The intrinsic alignment between halo major axes provides insight into structure growth and halo formation. Within hierarchical formation models, overdense regions of the density field collapse into sheets and filaments and underdense regions into voids. Dark matter haloes form at peaks of the density field which collapse and grow over time through mergers and smooth accretion.

Broadly speaking, the alignments that we have explored can be understood within the standard paradigm of hierarchical structure formation. Early-forming haloes collapse from peaks in the initial density field and form triaxial structures (Zel'dovich 1970). Tidal torquing then produces net halo angular momenta that are roughly orthogonal to halo major axes (Peebles 1969; White 1984). Those haloes which reside within larger-scale overdensities then merge to form larger haloes and so the population of massive haloes is built from mergers with smaller haloes. In the net, these mergers take place along strongly correlated directions (Zentner et al. 2005b; Libeskind et al. 2007, 2010). In particular, haloes preferentially merge along the filamentary structure. Sequences of mergers from preferential directions cause haloes to become elongated in the direction of the merger. As a result, host haloes tend to be prolate and their major axes tend to point along the filaments (Jing & Suto 2002; Bailin & Steinmetz 2005; Faltenbacher et al. 2005; Zentner et al. 2005b). The very same mergers supply host haloes with their subhaloes and the subhaloes tend to continue on elongated orbits that reflect the direction from which they merged (Zentner et al. 2005b). Of course, the details of these correlations must be computed from numerical simulations and many of the papers cited in this paragraph have done just that.

This overall picture is supported by observational studies. Halo ellipticity has now been detected via weak gravitational lensing and those lensing measurements also confirm that the major axes of galaxies must be correlated with the major axes of their host haloes. The non-zero ellipticities of haloes have been detected in both weak lensing (e.g. Evans & Bridle 2009; Clampitt & Jain 2016; Gonzalez et al. 2021; Robison et al. 2023) and strong lensing (e.g. Okabe et al. 2020). Moreover, these measurements are broadly consistent with theoretical expectations (e.g. Bett 2012; Velliscig et al. 2015; Chisari et al. 2017). Of particular interest in the current context are the results of Evans & Bridle (2009) and Gonzalez et al. (2021) who found that the orientation of the dark matter ellipse was correlated with the distribution of member galaxies in clusters. This suggests a detection of the bias for finding subhaloes to be aligned with the major axes of their host haloes. There are also a number of studies of SDSS data that show that satellite galaxies tend to reside along the major axes of their host galaxies (Brainerd 2005; Yang et al. 2006; Wang et al. 2018).

The alignment between host dark matter haloes and their subhaloes has implications for a variety of observations and particularly for the analysis of strong gravitational lensing. Strong gravitational lensing has become an indispensable probe of galaxy and halo structure. Among the most ambitious achievements and aims of strong lensing is to identify lensing features caused by subhaloes within a primary lens system and thereby constrain the properties of the dark matter. This can be done using flux-ratio anomalies (Mao & Schneider 1998; Metcalf & Madau 2001; Bradač et al. 2002; Dalal & Kochanek 2002; Metcalf & Zhao 2002; Keeton 2003; Metcalf et al. 2004; Treu & Marshall 2016; Gilman et al. 2018; Harvey et al. 2019; Treu, Suyu & Marshall 2022; Nierenberg et al. 2024; Zelko, Nierenberg & Treu 2024) and perturbations in lensing arcs (Meneghetti et al. 2006; Vegetti et al. 2010; Despali et al. 2018; Minor et al. 2021). In each

case, it is necessary to know the amount of substructure one should expect near the Einstein radius of the lens systems as viewed in projection along the line of sight.

We found that the number of subhaloes as well as the projected mass fraction in subhaloes is greater when viewed along a two-dimensional projection aligned with the major axis of the host halo. The mass fraction in subhaloes declines as the viewing angle with respect to the principle axis increases. The haloes themselves are typically nearly prolate ellipsoids, so the total mass density in projection is higher when viewed along a direction closely aligned with the major axis. This suggests that haloes may be more likely to serve as strong lenses when viewed at an angle nearly aligned with the major axis, though the strength of this preference depends upon the poorly constrained degree of alignment between the principle axes of a lens halo and the principle axes of the galaxy it hosts. Indeed, Hennawi et al. (2007) estimate that the mean value of the cosine of the viewing angle with respect to the major axis, $|\cos(\theta)|$, should be ~ 0.67 for multiply imaged systems, rather than 0.5, as would be expected if lensing probability were independent of viewing angle. There is a clear implication of these results. If haloes that serve as strong lenses are observed in projections that are nearly projections along the major axis, at least preferentially, then the expected mass fraction in subhaloes should be substantially larger than predictions for the global mass fraction in subhaloes. In follow-up work, we will explore the degree to which this potential bias can affect the interpretation of strong lensing observations and we advise those analysing strong lensing data to be aware of this potential bias.

There are possibly other important consequences of the alignments highlighted in this work. Our finding that subhalo and host halo angular momenta are aligned has consequences for galaxy formation studies. For example, it is common practice for semi-analytical galaxy formation models to adopt host halo angular momentum as a proxy for galaxy angular momentum either probabilistically (Somerville et al. 2008; Guo et al. 2011) or deterministically (Benson 2012). Interestingly, our results suggest that a large fraction of the net angular momentum of the host halo is carried by the subhaloes reside on orbits that are close to the plane of any galactic disc. Sufficiently large subhaloes will likely host their own galaxies. This provides an interesting contrast to a now well-known observation in the Local Group. The dwarf satellite galaxies of the Milky Way seem to orbit the Milky Way in a plane that is nearly *perpendicular* to the galaxy disc so that the angular momentum carried by the dwarf satellites is nearly perpendicular to that angular momentum of the Milky Way Galaxy (Kroupa et al. 2005; Pawlowski 2018). Satellites of Andromeda are found to be distributed anisotropically (Doliva-Dolinsky et al. 2023) and orbit the disc of Andromeda in a separate plane at a tilt of $\sim 50^\circ$ (Pawlowski 2018) with respect to the angular momentum of Andromeda. Such planar orbits of satellites have also been found in simulations using Milky Way and Andromeda Galaxy analogues in Santos-Santos et al. (2020) and Samuel et al. (2021) with the latter showing that they can exist in a plane perpendicular to the galactic disc. However, recent work indicates that the perpendicular alignment seen in the Milky Way could be temporary and due to a chance alignment with its two most distant satellites (Leo I and II) (Sales & Navarro 2023). Additionally, prior simulation work by Fielder et al. (2019) found host halo angular momentum to be the weakest indicator of subhalo abundance, further reinforcing the idea of alignment between host halo and subhalo angular momenta. All things considered, we believe that caution must be taken by galaxy formation studies when defining galaxy angular momentum.

In this paper, we provide a comprehensive look at the biased distribution of subhaloes about their host haloes. Using zoom-in simulations, we have shown that subhaloes are distributed anisotropically with respect to their host haloes. We find that (i) they are preferentially located along the major axis of their host halo and (ii) they orbit in a plane perpendicular to the spin axis of their host halo. These are effects that may be potentially important in galaxy formation models and, in particular, in the interpretation of strong lens systems.

ACKNOWLEDGEMENTS

We thank Atınç Çağan Şengül for insightful comments and helpful discussion that improved this manuscript.

This research made use of PYTHON, along with many community-developed or maintained software packages, including IPYTHON (Pérez & Granger 2007), JUPYTER (jupyter.org), MATPLOTLIB (Hunter 2007), NUMPY (van der Walt, Colbert & Varoquaux 2011), PANDAS (McKinney 2010), and SCIPY (Jones, Oliphant & Peterson 2001). This research made use of NASA's Astrophysics Data System for bibliographic information.

This work used data from the Symphony suite of simulations (http://web.stanford.edu/group/gfc/symphony/), which was supported by the Kavli Institute for Particle Astrophysics and Cosmology at Stanford University and SLAC National Accelerator Laboratory, and by the U.S. Department of Energy under contract number DE-AC02-76SF00515 to SLAC National Accelerator Laboratory.

DATA AVAILABILITY

The Symphony data products used in this work are publicly available at phil-mansfield.github.io/symphony.

REFERENCES

Alard C., 2008, MNRAS, 388, 375
Aragón-Calvo M. A., van de Weygaert R., Jones B. J. T., van der Hulst J. M., 2007, ApJ, 655, L5
Aubert D., Pichon C., Colombi S., 2004, MNRAS, 352, 376
Azzaro M., Patiri S. G., Prada F., Zentner A. R., 2007, MNRAS, 376, L43
Azzaro M., Zentner A. R., Prada F., Klypin A. A., 2006, ApJ, 645, 228
Bailin J., Steinmetz M., 2005, ApJ, 627, 647
Barnes J., Efstathiou G., 1987, ApJ, 319, 575
Becker M. R., 2015, preprint (arXiv:1507.03605)
Behroozi P. S., Wechsler R. H., Wu H.-Y., 2013, ApJ, 762, 109
Benson A. J., 2012, New Astron., 17, 175
Bett P., 2012, MNRAS, 420, 3303
Blumenthal G. R., Faber S. M., Primack J. R., Rees M. J., 1984, Nature, 311, 517
Bode P., Ostriker J. P., Turok N., 2001, ApJ, 556, 93
Bradač M., Schneider P., Steinmetz M., Lombardi M., King L. J., Porcas R., 2002, A&A, 388, 373
Brainerd T. G., 2005, ApJ, 628, L101
Brainerd T., Samuels A., 2021, in American Astronomical Society Meeting Abstracts. p. 156.02
Bullock J. S., 2010, preprint (arXiv:1009.4505)
Chiba T., Takahashi R., 2002, Prog. Theor. Phys., 107, 625
Chisari N. E. et al., 2017, MNRAS, 472, 1163
Clampitt J., Jain B., 2016, MNRAS, 457, 4135
Codis S., Pichon C., Devriendt J., Slyz A., Pogosyan D., Dubois Y., Sousbie T., 2012, MNRAS, 427, 3320
Colín P., Avila-Reese V., Valenzuela O., 2000, ApJ, 542, 622
Conn A. R. et al., 2013, ApJ, 766, 120
D'Onghia E., Burkert A., Murante G., Khochfar S., 2006, MNRAS, 372, 1525
Dalal N., Kochanek C. S., 2002, ApJ, 572, 25

Deason A. J. et al., 2011, MNRAS, 415, 2607
Despali G., Vegetti S., White S. D. M., Giocoli C., van den Bosch F. C., 2018, MNRAS, 475, 5424
Doliva-Dolinsky A. et al., 2023, ApJ, 952, 72
Dubinski J., 1994, ApJ, 431, 617
Dubinski J., Carlberg R. G., 1991, ApJ, 378, 496
Evans A. K. D., Bridle S., 2009, ApJ, 695, 1446
Faltenbacher A., Allgood B., Gottlöber S., Yepes G., Hoffman Y., 2005, MNRAS, 362, 1099
Faltenbacher A., Gottlöber S., Kerscher M., Müller V., 2002, A&A, 395, 1
Fielder C. E., Mao Y.-Y., Newman J. A., Zentner A. R., Licquia T. C., 2019, MNRAS, 486, 4545
Fielder C. E., Mao Y.-Y., Zentner A. R., Newman J. A., Wu H.-Y., Wechsler R. H., 2020, MNRAS, 499, 2426
Forero-Romero J. E., Contreras S., Padilla N., 2014, MNRAS, 443, 1090
Gilman D., Birrer S., Treu T., Keeton C. R., Nierenberg A., 2018, MNRAS, 481, 819
Gonzalez E. J., Makler M., García Lambas D., Chalela M., Pereira M. E. S., Van Waerbeke L., Shan H., Erben T., 2021, MNRAS, 501, 5239
Grebel E. K., 1999, in Whitelock P., Cannon C., eds, Proc. IAU Symp. 192, The Stellar Content of the Local Group. Astron. Soc. Pac., San Francisco, CA, p. 17
Guo Q. et al., 2011, MNRAS, 413, 101
Han C., Wang K., Avestruz C., Anbajagane D., 2023, preprint (arXiv:2312.08337)
Hartwick F. D. A., 2000, AJ, 119, 2248
Harvey D., Valkenburg W., Tamone A., Boyarsky A., Courbin F., Lovell M., 2019, MNRAS, 491, 4247
Hennawi J. F., Dalal N., Bode P., Ostriker J. P., 2007, ApJ, 654, 714
Hezaveh Y. D. et al., 2016, ApJ, 823, 37
Hoffmann K. et al., 2014, MNRAS, 442, 1197
Holmberg E., 1969, Ark. Astron., 5, 305
Hopkins P. F., Bahcall N. A., Bode P., 2005, ApJ, 618, 1
Hui L., 2021, ARA&A, 59, 247
Hunter J. D., 2007, Comput. Sci. Eng., 9, 90
Ibata R. A. et al., 2013, Nature, 493, 62
Ivezic Z. et al., 2019, ApJ, 873, 111
Jiang F., van den Bosch F. C., 2016, MNRAS, 458, 2848
Jing Y. P., 2002, MNRAS, 335, L89
Jing Y. P., Suto Y., 2002, ApJ, 574, 538
Jones E., Oliphant T., Peterson P., 2001, SciPy: open source scientific tools for Python. Available at: http://www.scipy.org/
Kang X., Wang P., 2015, ApJ, 813, 6
Karp J. S. M., Lange J. U., Wechsler R. H., 2023, ApJ, 949, L13
Kauffmann G., White S. D. M., Guiderdoni B., 1993, MNRAS, 264, 201
Kaufmann T., Mayer L., Wadsley J., Stadel J., Moore B., 2007, MNRAS, 375, 53
Keeton C. R., 2003, ApJ, 584, 664
Kiessling A. et al., 2015, Space Sci. Rev., 193, 67
Klypin A., Kravtsov A. V., Valenzuela O., Prada F., 1999, ApJ, 522, 82
Knebe A., Draganova N., Power C., Yepes G., Hoffman Y., Gottlöber S., Gibson B. K., 2008, MNRAS, 386, L52
Kroupa P., Theis C., Boily C. M., 2005, A&A, 431, 517
Kunkel W. E., Demers S., 1976, Royal Greenwich Observatory Bulletins, Number 182. The Galaxy and the Local Group. Royal Greenwich Observatory, Greenwich Park, p. 241
Lacey C., Cole S., 1994, MNRAS, 271, 676
Li C., Jing Y. P., Faltenbacher A., Wang J., 2013, ApJ, 770, L12
Libeskind N. I., Cole S., Frenk C. S., Okamoto T., Jenkins A., 2007, MNRAS, 374, 16
Libeskind N. I., Guo Q., Tempel E., Ibata R., 2016, ApJ, 830, 121
Libeskind N. I., Knebe A., Hoffman Y., Gottlöber S., Yepes G., Steinmetz M., 2010, MNRAS, 411, 1525
Libeskind N. I., Tempel E., Hoffman Y., Tully R. B., Courtois H., 2015, MNRAS, 453, L108
Lovell M. R., Frenk C. S., Eke V. R., Jenkins A., Gao L., Theuns T., 2014, MNRAS, 439, 300
Lynden-Bell D., 1976, MNRAS, 174, 695
Majewski S. R., 1994, ApJ, 431, L17
Mao S., Schneider P., 1998, MNRAS, 295, 587
Mao Y.-Y., Williamson M., Wechsler R. H., 2015, ApJ, 810, 21
Mateo M. L., 1998, ARA&A, 36, 435
Mckean J. et al., 2015, Proc. Sci., Strong Gravitational Lensing with the SKA. SISSA, Trieste, PoS#84
McKinney W., 2010, in van der Walt S., Millman J., eds, Proceedings of the 9th Python in Science Conference, Data Structures for Statistical Computing in Python. Austin,Texas, p. 56
Meneghetti M., Argazzi R., Pace F., Moscardini L., Dolag K., Bartelmann M., Li G., Oguri M., 2006, A&A, 461, 25
Metcalf R. B., Madau P., 2001, ApJ, 563, 9
Metcalf R. B., Moustakas L. A., Bunker A. J., Parry I. R., 2004, ApJ, 607, 43
Metcalf R. B., Zhao H., 2002, ApJ, 567, L5
Metz M., Kroupa P., Theis C., Hensler G., Jerjen H., 2009, ApJ, 697, 269
Mezini L., Fielder C. E., Zentner A. R., Mao Y.-Y., Wang K., Wu H.-Y., 2023, MNRAS, 526, 4157
Minor Q., Gad-Nasr S., Kaplinghat M., Vegetti S., 2021, MNRAS, 507, 1662
Moore B., Ghigna S., Governato F., Lake G., Quinn T., Stadel J., Tozzi P., 1999, ApJ, 524, L19
Morinaga Y., Ishiyama T., 2020, MNRAS, 495, 502
Nadler E. O. et al., 2023, ApJ, 945, 159
Navarro J. F., Benz W., 1991, ApJ, 380, 320
Navarro J. F., Steinmetz M., 1997, ApJ, 478, 13
Navarro J. F., White S. D. M., 1993, MNRAS, 265, 271
Nierenberg A. M. et al., 2024, MNRAS, 530, 2960
Oguri M. et al., 2012, MNRAS, 429, 482
Oguri M., Marshall P. J., 2010, MNRAS, 405, 2579
Okabe T. et al., 2020, MNRAS, 496, 2591
Pawlowski M. S., 2018, Mod. Phys. Lett. A, 33, 1830004
Pawlowski M. S., Pflamm-Altenburg J., Kroupa P., 2012, MNRAS, 423, 1109
Paz D. J., Stasyszyn F., Padilla N. D., 2008, MNRAS, 389, 1127
Peebles P. J. E., 1969, ApJ, 155, 393
Pérez F., Granger B. E., 2007, Comput. Sci. Eng., 9, 21
Peter A. H. G., Benson A. J., 2010, Phys. Rev. D, 82, 123521
Plionis M., Basilakos S., 2002, MNRAS, 329, L47
Porciani C., Dekel A., Hoffman Y., 2002a, MNRAS, 332, 325
Porciani C., Dekel A., Hoffman Y., 2002b, MNRAS, 332, 339
Robison B. et al., 2023, MNRAS, 523, 1614
Rodriguez F., Merchán M., Artale M. C., 2022, MNRAS, 514, 1077
Rodriguez F., Merchán M., Artale M. C., 2024, A&A, 688, A40
Sales L. V., Navarro J. F., 2023, Nat. Astron., 7, 376
Samuel J., Wetzel A., Chapman S., Tollerud E., Hopkins P. F., Boylan-Kolchin M., Bailin J., Faucher-Giguère C.-A., 2021, MNRAS, 504, 1379
Samuels A., Brainerd T. G., 2023, ApJ, 947, 56
Santos-Santos I. et al., 2020, ApJ, 897, 71
Schneider M. D., Frenk C. S., Cole S., 2012, J. Cosmol. Astropart. Phys., 2012, 030
Shao S., Cautun M., Frenk C. S., Grand R. J. J., Gómez F. A., Marinacci F., Simpson C. M., 2018, MNRAS, 476, 1796
Shaw L. D., Weller J., Ostriker J. P., Bode P., 2006, ApJ, 646, 815
Shi J., Wang H., Mo H. J., 2015, ApJ, 807, 37
Somerville R. S., Hopkins P. F., Cox T. J., Robertson B. E., Hernquist L., 2008, MNRAS, 391, 481
Springel V., White S. D. M., Hernquist L., 2004, The Shapes of Simulated Dark Matter Halos. International Astronomical Union Symposium, Sydney, Australia
Taylor J. E., Babul A., 2002, in Shanks T., Metcalfe N., eds, Proc. ASP Conf. Vol. 283, A New Era in Cosmology, A Semi-analytic Model of Halo Dynamics. Astron. Soc. Pac., San Francisco, p. 334
Taylor J. E., Babul A., 2004, MNRAS, 348, 811
Thomas P. A. et al., 1998, MNRAS, 296, 1061
Tormen G., 1997, MNRAS, 290, 411
Treu T., Marshall P. J., 2016, A&AR, 24, 11
Treu T., Suyu S. H., Marshall P. J., 2022, A&AR, 30, 8
Tulin S., Yu H.-B., 2018, Phys. Rep., 730, 1
van den Bosch F. C., Jiang F., 2016, MNRAS, 458, 2870

van der Walt S., Colbert S. C., Varoquaux G., 2011, Comput. Sci. Eng., 13, 22
Vegetti S., Koopmans L. V. E., Bolton A., Treu T., Gavazzi R., 2010, MNRAS, 408, 1969
Velliscig M. et al., 2015, MNRAS, 453, 721
Vera-Ciro C. A., Sales L. V., Helmi A., Frenk C. S., Navarro J. F., Springel V., Vogelsberger M., White S. D. M., 2011, MNRAS, 416, 1377
Wang H. Y., Jing Y. P., Mao S., Kang X., 2005, MNRAS, 364, 424
Wang M.-Y., Croft R. A. C., Peter A. H. G., Zentner A. R., Purcell C. W., 2013, Phys. Rev. D, 88, 123515
Wang M.-Y., Peter A. H. G., Strigari L. E., Zentner A. R., Arant B., Garrison-Kimmel S., Rocha M., 2014, MNRAS, 445, 614
Wang P., Luo Y., Kang X., Libeskind N. I., Wang L., Zhang Y., Tempel E., Guo Q., 2018, ApJ, 859, 115
Warren M. S., Quinn P. J., Salmon J. K., Zurek W. H., 1992, ApJ, 399, 405
Wechsler R. H., Bullock J. S., Primack J. R., Kravtsov A. V., Dekel A., 2002, ApJ, 568, 52
Welker C., Devriendt J., Dubois Y., Pichon C., Peirani S., 2014, MNRAS, 445, L46
White S. D. M., 1984, ApJ, 286, 38
White S. D. M., Rees M. J., 1978, MNRAS, 183, 341
Willman B., Governato F., Dalcanton J. J., Reed D., Quinn T., 2004, MNRAS, 353, 639
Wu H.-Y., Hahn O., Wechsler R. H., Mao Y.-Y., Behroozi P. S., 2013, ApJ, 763, 70
Xia Q., Kang X., Wang P., Luo Y., Yang X., Jing Y., Wang H., Mo H., 2017, ApJ, 848, 22
Yang X., Van Den Bosch F. C., Mo H. J., Mao S., Kang X., Weinmann S. M., Guo Y., Jing Y. P., 2006, MNRAS, 369, 1293
Zel'dovich Y. B., 1970, A&A, 5, 84
Zelko I. A., Nierenberg A. M., Treu T., 2024, MNRAS, 531, 885
Zentner A. R., Berlind A. A., Bullock J. S., Kravtsov A. V., Wechsler R. H., 2005a, ApJ, 624, 505
Zentner A. R., Bullock J. S., 2003, ApJ, 598, 49
Zentner A. R., Kravtsov A. V., Gnedin O. Y., Klypin A. A., 2005b, ApJ, 629, 219
Zhang Y., Yang X., Faltenbacher A., Springel V., Lin W., Wang H., 2009, ApJ, 706, 747

This paper has been typeset from a TEX/LATEX file prepared by the author.